2024 IEEE 63rd Conference on Decision and Control (CDC)
December 16-19, 2024. MiCo, Milan, Italy

Periodic Event-Triggered Boundary Control of Neuron Growth with Actuation at Soma

Cenk Demir[1], Mamadou Diagne[1] and Miroslav Krstic[1]

Abstract— **Exploring novel strategies for regulating axon growth, we introduce a periodic event-triggered control (PETC) to enhance the practical implementation of the associated PDE backstepping control law. Neurological injuries may impair neuronal function, but therapies like Chondroitinase ABC (ChABC) have shown promise in improving axon elongation by influencing the extracellular matrix. This matrix, composed of macromolecules and minerals, regulates tubulin concentration, potentially aiding neuronal recovery. The concentration and spatial distribution of tubulin influence axon elongation dynamics. Recent research explores feedback control strategies for this model, leading to the development of an event-triggering control (CETC). In this approach, the control law updates when the triggering condition is met, reducing actuation resource consumption. Through redesigning the triggering mechanism, we introduce PETC, updating control inputs at intervals but evaluating the event-trigger periodically, making it ideal for time-sliced actuators like ChABC. PETC is a step forward in designing feasible feedback laws for neuron growth. This strategy sets an upper bound on event triggers between periodic checks, ensuring convergence and preventing Zeno behavior. Through Lyapunov analysis, we demonstrate local exponential convergence of the system with PETC in the L^2-norm. Numerical examples confirm the theoretical findings.**

I. Introduction

Neurons, as fundamental components of neural networks, play a key role in sensory processing by transmitting electrical signals through their axons, which act like cellular wires. These axons contain tubulin proteins, essential for this communication process [30]. The dynamics of these proteins facilitate the elongation of axons, allowing them to reach the target neuron, establish synaptic connections, and complete the transmission process. However, neurological diseases or injuries can disrupt or completely halt this transmission such as Alzheimer's disease [23] and spinal cord injuries [22]. In such complications, neurons may degenerate, leading to axonal shrinkage or an inability to reach target neurons for signal transmission. Until recently, the prevailing belief was that injured neurons could not regenerate to complete the transmission process [16]. Recent research shows that regeneration is possible under certain conditions. Chondroitinase ABC therapy has demonstrated promising potential for stimulating neuron elongation [3].

Advancements in ChABC and other therapies may support neuron regeneration, but a key factor is the degree of neuronal elongation, controlled by tubulin dynamics. This process is modeled mathematically [12], [33], with a comprehensive model in [24] featuring a diffusion-reaction-advection PDE for tubulin evolution along the axon, paired with an ODE for tubulin at the growth cone and axon length. This model is a Stefan-type PDE, widely studied in the literature [13].

Partial differential equation (PDE) systems have attracted significant attention in control engineering. A pioneering research direction in this domain is boundary control of PDE systems which is based on the work [21]. Researchers have broadened their focus to include backstepping-based boundary control of various types of PDEs, systems that combine PDEs with ODEs, as well as systems that involve multiple interacting PDEs [20], [31], [32]. While previous studies focus on constant domain size in time, there are significant works on the global results of moving domains in time [8], [17]. This line of work has been extended to derive local stability results for moving boundary nonlinear hyperbolic PDEs [2], [4], [34]. Achieving stability for nonlinear parabolic PDEs with moving boundaries, especially without using the maximum principle, has been challenging until our recent study on axonal growth [5], [6].

While the control methods discussed operate continuously, some technologies require interventions only when necessary due to constraints in energy, communication, and computation [14]. This leads to event-triggered control, where actions are executed as needed to optimize resource usage. The concept was first developed for linear systems in [1], [15] and later extended to nonlinear systems in [18]. Building on these foundations, event-triggered boundary control for infinite-dimensional systems was proposed in [11]. Static and dynamic triggering mechanisms have been developed for ODEs and various classes of PDEs, specifically, for Stefan problem in [25], [26]. PETC and self-triggered control are proposed in [28] and [29], respectively, for a class of reaction-diffusion PDEs. Additionally, this method ensures safety and convergence to the set point of Stefan problems with actuator dynamics, as discussed in [19].

To address the neuron growth problem, a dynamic event-triggering mechanism for a coupled PDE-nonlinear ODE with a moving boundary is introduced in [7]. Given the feasibility challenges of real-time implementation in biological systems, we modify the continuous-time event-triggered control (CETC) by incorporating a periodic sampling rule. This introduces a dynamic periodic event-triggering control (PETC) approach, where the triggering function is only checked periodically while the control input is updated aperiodically. The PETC enhances the practical implementation of the control law by enabling its application to time-sliced

[1]Department of Mechanical and Aerospace Engineering, UC San Diego, 9500 Gilman Drive, La Jolla, CA, 92093-0411, cdemir@ucsd,edu, mdiagne@ucsd.edu, krstic@ucsd.edu

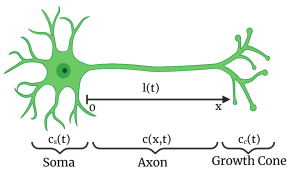

Fig. 1: Schematic of neuron and state variables

actuators like ChABC for axon growth. The strategy derives a new triggering condition and sets an upper bound on the event trigger between periodic checks, defined as the sampling period. Our study differs from [27], which used observer-based PETC for the one-phase Stefan problem. While the outcome in [27] pertains to a system exhibiting *geometric nonlinearity,* the neuron growth process involves both *geometrical and analytical nonlinearities* leading to a *local* convergence result. The PETC boundary controller guarantees L^2 local exponential convergence in closed-loop.

The paper is structured as follows: Section II details the axon growth model, reference error analysis, and control law. Section III reviews the event-triggering mechanism and prior results. Section IV introduces a new periodic event-triggering control, and Section V presents simulations.

II. Tubulin-Driven Axon Growth Modeling and Control

This section presents the tubulin-driven axonal growth model and a boundary control law.

A. Understanding axon growth

1) A model with a moving boundary PDE: Tubulin, a group of proteins, drives the development of a newly formed axon. Assuming unattached tubulin molecules along the axon are negligible and that only tubulin contributes to axon growth, the evolution of this process in time and space can be modeled as follows [9], [10].

$$c_t(x,t) = Dc_{xx}(x,t) - ac_x(x,t) - gc(x,t), \tag{1}$$

$$c_x(0,t) + c(0,t) = -q_{\rm s}(t), \tag{2}$$

$$c(l(t),t) = c_{\rm c}(t), \tag{3}$$

$$\dot{c}_{\rm c}(t) = \tilde{a}c_{\rm c}(t) - \beta c_x(l(t),t) - \kappa c_{\rm c}^2(t) + c_\infty \tilde{r}_{\rm g}, \tag{4}$$

$$\dot{l}(t) = r_{\rm g}(c_{\rm c}(t) - c_\infty) \tag{5}$$

where the constants in (4) are

$$\tilde{a}_1 = \frac{a - r_{\rm g}c_\infty}{l_{\rm c}} - g - \tilde{r}_{\rm g}, \quad \beta = \frac{D}{l_{\rm c}}, \quad \kappa = \frac{r_{\rm g}}{l_{\rm c}}. \tag{6}$$

In this model, $c(x,t)$ is the tubulin concentration in the axon, varying with space x time t, while q represents the combined tubulin flux and concentration at soma. The axon length is denoted $l(t)$, which is the distance between the soma and the growth cone. The subscripts s and c are used for the soma and the growth cone, respectively, as shown in Fig. 1. The parameters, D, a, and g are tubulin diffusivity, velocity, and degradation constants, respectively. The parameters in (4) and (5) include $l_{\rm c}$ representing the growth ratio, $\tilde{r}_{\rm g}$ denoting the reaction rate of the microtubules production process, c_∞ as the equilibrium of tubulin concentration in the cone, and $r_{\rm g}$ serving as a lumped parameter. Detailed descriptions and derivations of $r_{\rm g}$ and other parameters are available in [10].

2) The steady-state solution and reference error system: We derive a steady-state solution for the concentration, corresponding to a desired axon length $l_{\rm s}$. The steady-state spatially distributed steady-state tubulin concentration is

$$c_{\rm eq}(x) = c_\infty \left(K_+ e^{\lambda_+(x-l_{\rm s})} + K_- e^{\lambda_-(x-l_{\rm s})}\right), \tag{7}$$

where

$$\lambda_\pm = \frac{a \pm \sqrt{a^2+4Dg}}{2D}, \quad K_\pm = \frac{1}{2} \pm \frac{a - 2gl_{\rm c}}{2\sqrt{a^2+4Dg}}, \tag{8}$$

and the steady-state input for the combination of tubulin flux and concentration in the soma is

$$q_{\rm s}^* = -c_\infty \left(K_+(1+\lambda_+)e^{-\lambda_+ l_{\rm s}} + K_-(1+\lambda_-)e^{-\lambda_- l_{\rm s}}\right). \tag{9}$$

The reference error system relative to (1)-(5) is given by the dynamics of errors given below

$$u_t(x,t) = Du_{xx}(x,t) - au_x(x,t) - gu(x,t), \tag{10}$$

$$u_x(0,t) + u(0,t) = U(t), \tag{11}$$

$$u(l(t),t) = h^*(X(t)), \tag{12}$$

$$\dot{X}(t) = AX(t) + f(X(t)) + Bu_x(l(t),t), \tag{13}$$

where the reference error states, $u(x,t)$, $z_1(t)$ and $z_2(t)$, and the reference error input $U(t)$ are defined as

$$u(x,t) = c(x,t) - c_{\rm eq}(x), \quad U(t) = -(q_{\rm s}(t) - q_{\rm s}^*) \tag{14}$$

$$z_1(t) = c_{\rm c}(t) - c_\infty, \quad z_2(t) = l(t) - l_{\rm s}. \tag{15}$$

X is a state vector in $\mathbb{R}^2$, given as $X(t) = [z_1(t) \quad z_2(t)]^\top$. The parameters and the functions in (10)-(13) are defined as:

$$A = \begin{bmatrix} \tilde{a}_1 & -\beta\tilde{a}_2 \\ r_{\rm g} & 0 \end{bmatrix}, \quad B = \begin{bmatrix} -\beta \\ 0 \end{bmatrix}, \tag{16}$$

$$f(X(t)) = -\kappa z_1^2(t) + \beta f_1(z_2(t)), \tag{17}$$

$$h^*(X) = z_1(t) + c_\infty - c_\infty(K_+ e^{\lambda_+ z_2(t)} + K_- e^{\lambda_- z_2(t)}), \tag{18}$$

$$\tilde{a}_2 = c_\infty \left(\lambda_+^2 K_+ + \lambda_-^2 K_-\right), \tag{19}$$

$$f_1(z_2(t)) = -c_\infty K_+ \lambda_+ e^{\lambda_+ z_2(t)} - c_\infty K_- \lambda_- e^{\lambda_- z_2(t)} + \tilde{a}_2 z_2(t) + c_\infty \frac{a - gl_{\rm c}}{D}. \tag{20}$$

B. Control Law Design

1) Linearization of the finite-dimensional part of the cascade system : We begin by linearizing the nonlinear ODEs defined in (13) around zero states:

$$u_t(x,t) = Du_{xx}(x,t) - au(x,t) - gu(x,t), \tag{21}$$

$$u_x(0,t) + u(0,t) = U(t), \tag{22}$$

$$u(l(t),t) = H^\top X(t), \tag{23}$$

$$\dot{X}(t) = A_1 X(t) + Bu_x(l(t),t), \tag{24}$$

where the vector $H \in \mathbb{R}^2$ is defined as

$$A_1 = \begin{bmatrix} \tilde{a}_1 & \tilde{a}_3 \\ r_{\rm g} & 0 \end{bmatrix}, \quad H = \begin{bmatrix} 1 & -\frac{(a - gl_{\rm c})c_\infty}{D} \end{bmatrix}^\top, \tag{25}$$

where $\tilde{a}_3 = \frac{a^2+Dg-agl_{\rm c}}{D^2}$. By applying the following backstepping transformation

$$w(x,t) = u(x,t) - \int_x^{l(t)} k(x,y)u(y,t)dy - \phi(x - l(t))^\top X(t), \tag{26}$$

we can map the linearized reference error system to a desired target system which is

$$w_t(x,t) = Dw_{xx}(x,t) - aw_x(x,t) - gw(x,t) - \dot{l}(t)F(x,X(t)), \tag{27}$$

$$w_x(0,t) + w(0,t) = -\frac{1}{D}(H - \epsilon)^\top Bu(0,t), \tag{28}$$

$$w(l(t),t) = \epsilon^\top X(t), \tag{29}$$

$$\dot{X}(t) = (A_1 + BK^\top)X(t) + Bw_x(l(t),t), \tag{30}$$

with the redundant nonlinear term is described as $F(x, X(t)) = \left(\phi'(x - l(t))^T - k(x, l(t))C^T\right) X(t)$ where $K \in \mathbb{R}^2$ is chosen as

$$k_1 > \frac{\tilde{a}_1}{\beta}, \quad k_2 > \frac{\tilde{a}_3}{\beta}. \tag{31}$$

to make $A_1 + BK$ Hurwitz and $\epsilon \in \mathbb{R}^2$ will be chosen in the stability analysis.

The approach for obtaining gain kernels in (26), namely $k(x, y)$ and $\phi(x)$, is detailed in [5]. Simply, $k(x, y)$ and $\phi(x)$ are obtained as:

$$k(x,y) = -\frac{1}{D}\phi(x-y)^\top B, \tag{32}$$

$$\phi(x)^\top = \left[(H-\epsilon)^\top \quad K^\top - \tfrac{1}{D}H^\top BH^\top\right] e^{N_1 x}\begin{bmatrix} I \\ 0 \end{bmatrix}, \tag{33}$$

where the matrix $N_1 \in R^{4\times 4}$ is defined as

$$N_1 = \begin{bmatrix} 0 & \frac{1}{D}\left(gI + A + \frac{a}{D}BH^\top\right) \\ I & \frac{1}{D}\left(BH^\top + aI\right) \end{bmatrix}. \tag{34}$$

The inverse transformation is given in [7] and detailed solutions for the gain kernels are provided in [5].

2) Continuous-time and sampled-data control law: By taking the spatial derivative of the transformation and substituting $x = 0$ into both the backstepping transformation and its spatial derivative, and setting boundary condition (28), the control law is derived as

$$U(t) = -\frac{1}{D}\int_0^{l(t)} p(x)Bu(x,t)dx + p(l(t))X(t), \tag{35}$$

where

$$p(x) = \phi'(-x)^\top + \phi(-x)^\top. \tag{36}$$

The system outlined in (1)-(5), with the continuous-time controller input (35), is locally exponentially stable in the L^2-norm sense, as demonstrated in [7]. To develop the periodic event-triggered control mechanism, the CTC input is sampled at discrete intervals, which holds it constant between events. This approach yields the following sampled-data control.

$$U_k^\omega(t) := U(t_k^\omega), \tag{37}$$

where is employed at

$$u_x(0,t) + u(0,t) = U_k^\omega(t). \tag{38}$$

for $\forall t \in [t_k^\omega, t_{k+1}^\omega)$, $k \in \mathbb{N}$ with the increasing time sequence, $I^\omega = \{t_k^\omega\}_{k\in\mathbb{N}}$, where $t_0^\omega = 0$ and $\omega = \{\text{“}c\text{”}, \text{“}p\text{”}\}$. The notations “$c$” and “$p$” represent CETC and PETC, respectively. The control input is sampled from (35) at each sampling time, emulating the continuous-time controller with a Zero-Order Hold.

III. Continuous-time Event Triggered control

In this section, we provide a summary of a CETC design detailed in [7].

Definition 1: Continuous-time event-triggering consists of two stages: the occurrence of the event and the application of the control signal when the event occurs. Detection of the time is defined as

$$t_{k+1}^c = \inf\{t \in R_+ | t > t_k^c \wedge d^2(t) > -\gamma m(t)\} \tag{39}$$

for all $t \in [t_k^c, t_{k+1}^c)$, $d(t)$ is given as

$$d(t) = U(t) - U_k^c(t) \tag{40}$$

and $m(t)$ satisfies the ODE

$$\begin{aligned}\dot{m}(t) = &-\eta m(t) + \rho d(t)^2 - \beta_1 X(t)^2 - \beta_2 X(t)^4 \\ &- \beta_3 X(t)^6 - \beta_4 |w(0,t)|^2 - \beta_5 ||w(x,t))||^2.\end{aligned} \tag{41}$$

The event-triggering design parameters are $\sigma \in (0,1)$, $\gamma > 0$, $\eta > 0$, and β_i and ρ are selected according to the specifications outlined in [7] as

$$\rho \geq \frac{d_1^2}{2D}, \quad \beta_i = \frac{\alpha_i}{\gamma(1-\sigma)}. \tag{42}$$

Remark 1: The triggering mechanism defined by (39) and (41) has the property of $d^2(t) \leq \gamma m(t)$ and $m(t) > 0$, $\forall\ t \in [0, \sup\{I^c\})$ as detailed in [7].

Remark 2: Considering the increasing set of event-times $\{t_k^c\}_{k\in\mathbb{N}}$ with $t_0 = 0$, the following bound is obtained for the time derivative of the input holding error

$$\begin{aligned}\dot{d}^2(t) \leq &\rho_1 d^2(t) + \alpha_1 X(t)^2 + \alpha_2 X(t)^4 + \alpha_3 X(t)^6 \\ &+ \alpha_4 w(0,t)^2 + \alpha_5 ||w(x,t)||^2,\end{aligned} \tag{43}$$

where the parameters, $\rho_1, \alpha_1, \alpha_2, \alpha_3, \alpha_4, \alpha_5$ are given in [7], equations (50)-(57).

Theorem 1: [7] For the event-triggered mechanism described in (37)-(39), the set of event-times $\{t_k^c\}_{k\in\mathbb{N}}$ ensures that the function $\Gamma^c(t) := d(t)^2 - \gamma m(t)$ remains non-positive for all $t \in [t_k^c, t_{k+1}^c)$, where $k \in \mathbb{N}$.

The proof of this theorem and the following results are given in [7] and the following hold:

1) The set of event-times $\{t_k^c\}_{k\in\mathbb{N}}$ with triggering mechanism (37)-(39) and with the design parameters specified in [7], ensures that Zeno behavior does not occur. This is because there exists a minimal dwell-time, $\tau > 0$, between two execution times, given by
$$\tau = \int_0^1 \frac{1}{a_1 s^2 + a_2 s + a_3} ds, \tag{44}$$
where
$$a_1 = \rho\sigma\gamma > 0, \tag{45}$$
$$a_2 = 1 + 2\rho_1 + (1-\sigma)\rho + \eta > 0, \tag{46}$$
$$a_3 = (1 + \rho_1 + \gamma(1-\sigma)\rho + \eta)\frac{1-\sigma}{\sigma} > 0. \tag{47}$$
2) Given an initial condition $m(0) < 0$, the variable $m(t)$ governed by (41), satisfies $m(t) < 0$ for all $t > 0$.
3) The closed-loop system (1)-(5), along with the event-triggered mechanism (37), locally exponentially converges to the desired axon length in the L^2-sense.

In the next section, we propose a periodic event-triggering mechanism.

IV. Periodic Event Triggering Mechanism

In this section, we propose a periodic event-triggering mechanism for axonal growth.

Definition 2: Consider the event-triggering function $\Gamma^p(t)$, which undergoes periodic evaluation with a period of $h > 0$. The PETC that generates the events are characterized by two parts. The event-trigger mechanism which is a periodic event-

trigger that determines the event times

$$t_{k+1}^p = \inf\{t \in \mathbb{R}_+ | t > t_k^p,\ \Gamma^p(t) > 0,\ t = nh, \\ h > 0,\ n \in \mathbb{N}\}, \tag{48}$$

with $t_0^p = 0$ where h is sampling period and

$$\Gamma^p(t) = \upsilon_1 d^2(t) - \upsilon_2 m(t) \tag{49}$$

where $\upsilon_1 > 0$ and $\upsilon_2 > 0$. The feedback control law that is derived as

$$U_k^p(t) = -\frac{1}{D}\int_0^{l(t_k^p)} p(x)Bu(x,t_k^p)dx + p(l(t_k^p))X(t_k^p) \tag{50}$$

for all $t \in [t_k^p, t_{k+1}^p)$ for $k \in \mathbb{N}$.

Note that periodicity in the triggering conditions (48), allows us to monitor the triggering function *periodically* and update the control laws *aperiodically,* removing the continuous monitoring of the PDE-ODE state variables. Then, the boundary condition (11) becomes

$$u_x(0,t) + u(0,t) = U(t_k^p). \tag{51}$$

A. Design of the periodic event triggering function $\Gamma^p(t)$

Selection of the sampling period. The sampling period, denoted as h, represents the unit of time during which the control input is updated. Let the periodic event-triggered function given by (48), along with the boundary condition in (51) and the plant dynamics from (1)-(5), satisfy the condition $\Gamma^p(t) \leq 0$ for all t within the interval $t \in [t_k^p, t_{k+1}^p)$ for $k \in \mathbb{N}$. Hence, it follows that $m(t) < 0$ for all $t > 0$. The parameter h is selected to satisfy

$$0 < h \leq \tau, \tag{52}$$

where the upper bound, τ, is the minimum inter-event time of the CETC design defined in (44)-(47).

Proposition 1: Under the definition of the periodic event-triggered boundary control (51), with the sampling period $h < \tau$, it holds that

$$\Gamma^c(t) \leq \frac{1}{q}(a+\gamma\rho)d^2(nh)e^{q(t-nh)} - \frac{1}{q}\gamma\rho d^2(nh) \\ + \frac{1}{q}q\gamma m(nh)e^{-\eta(t-nh)}, \tag{53}$$

for all $t \in [nh, (n+1)h)$ and any $n \in [t_k^p/h, t_{k+1}^p/h) \subset \mathbb{N}$, where $q = 1+\eta+\rho_1$ and $\Gamma^c(t) = d^2(t) - \gamma m(t)$ for $\gamma > 0$.

Proof. Taking the time derivative of $\Gamma^c(t)$ in $t \in [nh, (n+1)h)$ and $n \in [t_k^p/h, t_{k+1}^p/h) \subset \mathbb{N}$, one can show that

$$\dot{\Gamma}^c(t) \leq d^2(t) + \dot{d}^2(t) - \gamma\dot{m}(t). \tag{54}$$

Since $m(t)$ satisfies Remark 1 and (1)-(5) with the event-triggered control law (37) is locally exponentially convergent, (54) exhibit smooth behavior in the interval $t \in [nh, (n+1)h)$ and for any $n \in [t_k^p/h, t_{k+1}^p/h) \subset \mathbb{N}$. Using Lemma 1 and the definition of $\Gamma^c(t)$, we establish the existence of a non-negative function $\iota(t) \in C^0((t_k^p, t_{k+1}^p); \mathbb{R}_+)$ such that:

$$\dot{\Gamma}^c(t) = (1+\rho_1+\gamma\rho)\Gamma(t) - (\gamma\beta_1 - \alpha_1)X(t)^2 \\ - (\gamma\beta_2 - \alpha_2)X(t)^4 - (\gamma\beta_3 - \alpha_3)X(t)^6 \\ - (\gamma\beta_4 - \alpha_4)u(0,t)^2 - (\gamma\beta_5 - \alpha_5)||u(x,t)||^2 \\ + ((1+\rho_1+\gamma\rho)\gamma + \eta\gamma)m(t) - \iota(t), \tag{55}$$

for all $t \in [nh, (n+1)h)$ and for any $n \in [t_k^p/h, t_{k+1}^p/h) \subset \mathbb{N}$. Moreover, through the substitution of $d^2(t) = \Gamma^c(t) + \gamma m(t)$, we can use the dynamics of $m(t)$ and obtain the solution of $m(t)$ and $\Gamma^c(t)$ system of ODEs. Since we have the following relationship

$$1 + \eta + 7|p(0)B|^2 > 0, \tag{56}$$

Ascending order of triggering times that is the solution of (44) is represented by

$$\tau = \frac{1}{q}\ln\left(1 + \frac{\sigma q}{(1-\sigma)(q+\gamma\rho)}\right), \tag{57}$$

where $q = 1+\eta+\rho_1$. By using the solution of $\Gamma^c(t)$, we can derive the following expression for $t \in [nh, (n+1)h)$:

$$\Gamma^c(t) \leq \frac{1}{q}\left(-\gamma(q+\gamma\rho)m(nh) - \gamma\rho\Gamma^c(nh) \right. \\ \left. + (q+\gamma\rho)\left(\Gamma^c(nh) + \gamma m(nh)\right)e^{q(t-nh)}\right). \tag{58}$$

Upon performing the substitution $\Gamma^c(nh)$ into (58), we are able to derive the inequality (53) which is valid for all $t \in [nh, (n+1)h)$. This concludes the proof. □

Building upon Lemma 2, the update time for the control input can be determined by identifying when the subsequent condition is met for any $t \in [nh, (n+1)h)$, thereby challenging the positive definiteness of $\Gamma^c(t)$.

$$(q+\gamma\rho)d^2(nh)e^{q(t-nh)} - \gamma\rho d^2(nh) + q\gamma m(nh) > 0, \tag{59}$$

Thus, one can choose this condition as $\Gamma^p(t)$ such that

$$\Gamma^p(t) = (q+\gamma\rho)e^{qh}d^2(t) - \gamma\rho d^2(t) + q\gamma m(t), \tag{60}$$

which completes the design process.

Theorem 2: Let the design parameters, ρ, ρ_1 and β_i as defined in [7], set the sampling rate in accordance with (52), let $\gamma, \eta > 0$ and $\sigma \in (0,1)$. Let us consider the periodic event-triggering mechanism (48)-(50) with the $\Gamma^p(t)$ as defined in (60) which generates the increasing sequence of times $\{t_k^p\}_{k\in\mathbb{N}}$ with $t_0^p = 0$. Then, for $\Gamma^c(t)$ and $m(t)$ with $m(t) > 0$, it holds that $\Gamma^c(t) \leq 0$ and $m(t) > 0$ for all $t > 0$.

Proof. Due to space constraints, we omit this proof, which can be stated following the proof of Theorem 2 in [28]. □

B. Local exponential convergence under PETC

In order to prove that the closed-loop system (1)-(5) with the control law (37) and the periodic event-triggering mechanism (48) and (60), is locally exponentially convergent, we first obtain the following target system by applying transformation (26)

$$w_t(x,t) = Dw_{xx}(x,t) - aw_x(x,t) - gw(x,t) - \dot{l}(t)F(x,X(t)) \\ - \phi(x-l(t))^\top f(X(t)) - G(x,l(t))h^*(X), \tag{61}$$

$$w_x(0,t) + w(0,t) = d(t) - \frac{1}{D}(H-\epsilon)^\top Bu(0,t), \tag{62}$$

$$w(l(t),t) = h^*(X(t)) + \epsilon^\top X(t), \tag{63}$$

$$\dot{X}(t) = (A+BK)X(t) + f(X(t)) + Bw_x(l(t),t), \tag{64}$$

where $G(x,l(t)) := \left(\phi'(x-l(t))^\top + \frac{a}{D}\phi(x-l(t))^\top\right)B$. Using the transformation below

$$\varpi(x,t) = w(x,t) - h^*(X(t)) \tag{65}$$

converts (61)-(64) into

$$\varpi_t(x,t) = D\varpi_{xx}(x,t) - a\varpi_x(x,t) - g\varpi(x,t) \\ + gh^*(X(t)) - \dot{l}(t)F(x,X(t)) - \dot{h}^*(X(t))B\varpi_x(l(t),t) \\ - \phi(x-l(t))^\top f(X(t)) - G(x,l(t))h^*(X)$$

$$- \dot{h}^*(X(t))\left((A+BK)X(t)+f(X(t))\right), \tag{66}$$

$$\varpi_x(0,t)+\varpi(0,t)=d(t)-\frac{1}{D}\left(H-\epsilon\right)^\top Bu(0,t) + h^*(X(t)), \tag{67}$$

$$\varpi(l(t),t)=\epsilon^\top X(t), \tag{68}$$

$$\dot{X}(t)=(A+BK)X(t)+f(X(t))+B\varpi_x(l(t),t). \tag{69}$$

Below, we state the convergence result.

Theorem 3: Let the design parameters, ρ, ρ_1 and β_i given as defined in Theorem 2. Consider the periodic event-triggering rule (48)-(50) with the periodic event-triggering function (60) and sampling rate h defined in (52), which generates an increasing event-times $\{t_k^p\}_{k\in\mathbb{N}}$. Assuming the well-posedness, the closed-loop system of (1)-(5) with the boundary control law (60) and (36) is locally exponentially convergent in L^2-norm sense.

Proof. To demonstrate local convergence, we first establish the system's properties in a non-constant spatial interval, as derived in [7]:

$$0<l(t)\leq \bar{l}, \quad |\dot{l}(t)|\leq \bar{v} \tag{70}$$

for some $\bar{l}>l_s>0$ and $\bar{v}=\frac{D}{16(D+1)}$. As demonstrated in Theorem 2 of [7], $m(t)<0$ for all $t\in[t_k^p,t_{k+1}^p)$ where $k\in\mathbb{N}$, implying $\Gamma^c(t)\leq 0$ for $t\in[t_k^p,t_{k+1}^p)$. Assuming the well-posedness of the closed-loop system and following the methodology outlined in [7], the subsequent Lyapunov functional is considered

$$V(t)=V_1(t)-m(t), \tag{71}$$

where

$$V_1(t)=d_1\frac{1}{2}\int_0^{l(t)}\varpi(x,t)^2dx+X(t)^\top\left(d_2P_1+\frac{1}{2}P_2\right)X(t) \tag{72}$$

and $d_1>0$, $d_2>0$, $P_1\succ 0$ and $P_2\succeq 0$ are positive definite and positive semidefinite matrices satisfying the Lyapunov equations:

$$(A+BK^\top)^\top P_1+P_1(A+BK^\top)=-Q_1,$$

$$(A+BK^\top)^\top(P_1+P_2)+(P_1+P_2)(A+BK^\top)=-Q_2$$

where

$$P_1=\begin{bmatrix}p_{1,1}&p_{1,2}\\p_{1,2}&p_{2,2}\end{bmatrix}, \quad P_2=\begin{bmatrix}\frac{D\epsilon_1}{\beta}-2p_{1,1}&0\\0&0\end{bmatrix} \tag{73}$$

where we pick $\epsilon\in\mathbb{R}^2$ as $\epsilon_1\geq 2l_cp_{1,1}$ and $\epsilon_2=\frac{p_{1,2}}{l_cd_1}$ for some positive definite matrices $Q_1\succ 0$ and $Q_2\succ 0$. By taking the time derivative of (72), applying Poincaré's, Agmon's, and Young's inequalities, we derive the following expression:

$$\dot{V}\leq -\alpha^*V+\xi_1V^{3/2}+\xi_2V^2+\xi_3V^{5/2}+\xi_4V^3 \tag{74}$$

where α^*, ξ_i, d_1 and d_2 are given in [7]. By following Lemma 3, Lemma 4 and Lemma 5 in [7], one can conclude

$$V_1(t)-m(t)\leq e^{-\alpha^*t}V(0) \tag{75}$$

by applying the comparison principle one can obtain the following norm estimate for the target system (ϖ,X):

$$\begin{aligned}&d_1\frac{1}{2}||\varpi(x)||^2+d_2X(t)^\top\left(P_1+\frac{1}{d_2}P_2\right)X(t)\\ \leq& e^{-\alpha^*t}\left(\frac{d_1}{2}||\varpi(0)||^2+d_2X(0)^\top\left(P_1+\frac{1}{d_2}P_2\right)X(0)\right)\\ &-e^{-\alpha^*t}m(0)\end{aligned} \tag{76}$$

Using the invertibility of the transformation (65), we prove the target system (w,X) is locally exponentially convergent.

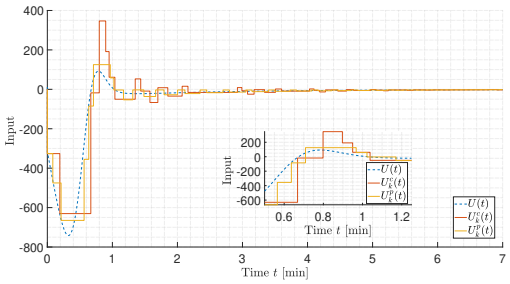

Fig. 2: Comparison between periodic-event triggering control input $U_k^p(t)$, continuous time event triggering control input $U_k^c(t)$ and the continuous control law $U(t)$

For the original system (u,X), the invertibility of the back-stepping transformation (26) leads to the same conclusion for the closed-loop system. This completes the proof. □

V. Numerical Simulations

In this section, we simulate the system from equations (1)-(5), employing the control law (35) along with the designed periodic event-triggering mechanism (48) utilizing the triggering function (60). The model parameters are detailed in Table I. Initial conditions are specified as $c_0(x)=1.5c_\infty$ for the tubulin concentration along the axon and $l_0=1\mu m$ for the initial axon length. Control gain parameters are set as $k_1=-0.001$ and $k_2=3\times10^{13}$. The event-triggering parameters are set as follows $m(0)=-0.5$, $\beta_1=2.5\times10^8$, $\beta_2=8\times10^9$, $\beta_3=1\times10^{11}$, $\beta_4=4\times10^{11}$, $\beta_5=4.5\times10^{11}$, $\rho=1.5\times10^{-15}$, $\gamma=1$, $\eta=2$ and $\sigma=0.8$. Moreover, the sampling period for the periodic event-triggering mechanism is selected as $h=0.5\ ms$ which is smaller than the minimal dwell time $\tau\approx 0.54\ ms$.

Fig. 2 illustrates the evolution of the continuous-time control input, $U(t)$, the event-triggering control input, $U_k^c(t)$, as defined in (37) with the triggering mechanism given by (39)-(41), and the periodic event-triggering control input, $U_k^p(t)$, as defined in (50) with the triggering condition in (48) and triggering function in (60). While PETC closely emulates the CETC control input behavior, both PETC and CETC minimized the necessity of control law updates by maintaining comparable performance. In Fig. 3, tubulin concentration, $c(x,t)$, and axon length, $l(t)$, converge to the steady-state solution. Note that tubulin concentration changes more smoothly with the PETC mechanism compared to the CETC mechanism, improving practical applicability.

VI. Conclusion

This paper proposes a periodic event-triggering control for the axonal growth problem, modeled as coupled PDE and nonlinear ODE. The approach uses sampled-data control,

TABLE I: Biological constants and control parameters

Parameter	Value	Parameter	Value
D	$10\times10^{-12}m^2/s$	$\tilde{r}_g$	0.053
a	$1\times10^{-8}m/s$	γ	10^4
g	$5\times10^{-7}\ s^{-1}$	l_c	$4\mu m$
r_g	$1.783\times10^{-5}\ m^4/(mols)$	l_s	$12\mu m$
c_∞	$0.0119\ mol/m^3$	l_0	$1\mu m$

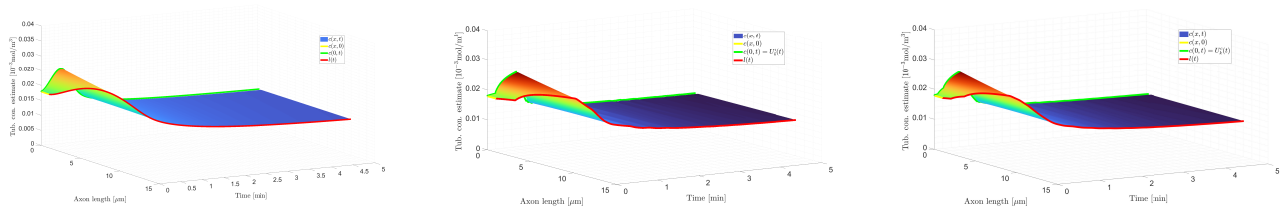

(a) Continous time control input. (b) Event-triggered control input. (c) Periodic event-triggered control input.

Fig. 3: The tubulin concentration, $c(x,t)$, reaches steady-state, $c_{\text{eq}}(t)$, by about $t = 4.5$ minutes for continuous control, CETC, and PETC. Axon length, $l(t)$, converges to the target, l_s, by around $t = 4$ minutes for all sampling methods.

requiring only periodic monitoring and aperiodic updates. Future work will focus on adaptive control and parameter estimation, with Batch Least Squares Identifiers (BaLSI) offering potential for finite-time identification and local exponential convergence.

Acknowledgements

The authors express appreciation to Bhathiya Rathnayake for engaging in generous and selfless discussions on event-triggered control.

References

[1] K.-E. Åarzén, "A simple event-based pid controller," *IFAC Proceedings Volumes*, vol. 32, no. 2, pp. 8687–8692, 1999.

[2] G. Bastin, J.-M. Coron, A. Hayat, and P. Shang, "Boundary feedback stabilization of hydraulic jumps," *IFAC Journal of Systems and Control*, vol. 7, p. 100026, 2019.

[3] E. J. Bradbury and L. M. Carter, "Manipulating the glial scar: chondroitinase ABC as a therapy for spinal cord injury," *Brain research bulletin*, vol. 84, no. 4-5, pp. 306–316, 2011.

[4] M. Buisson-Fenet, S. Koga, and M. Krstic, "Control of piston position in inviscid gas by bilateral boundary actuation," in *2018 IEEE Conference on Decision and Control (CDC)*. IEEE, 2018, pp. 5622–5627.

[5] C. Demir, S. Koga, and M. Krstic, "Neuron growth control by pde backstepping: Axon length regulation by tubulin flux actuation in soma," in *2021 60th IEEE Conference on Decision and Control (CDC)*, 2021, pp. 649–654.

[6] ——, "Neuron growth output-feedback control by pde backstepping," in *2022 American Control Conference (ACC)*. IEEE, 2022, pp. 4159–4164.

[7] ——, "Event-triggered control of neuron growth with actuation at soma," in *2024 American Control Conference (ACC)*. IEEE, 2024, pp. 5301–5306.

[8] M. Diagne, P. Shang, and Z. Wang, "Feedback stabilization for the mass balance equations of an extrusion process," *IEEE Transactions on Automatic Control*, vol. 61, no. 3, pp. 760–765, 2015.

[9] S. Diehl, E. Henningsson, and A. Heyden, "Efficient simulations of tubulin-driven axonal growth," *Journal of computational neuroscience*, vol. 41, no. 1, pp. 45–63, 2016.

[10] S. Diehl, E. Henningsson, A. Heyden, and S. Perna, "A one-dimensional moving-boundary model for tubulin-driven axonal growth," *Journal of theoretical biology*, vol. 358, pp. 194–207, 2014.

[11] N. Espitia, A. Girard, N. Marchand, and C. Prieur, "Event-based control of linear hyperbolic systems of conservation laws," *Automatica*, vol. 70, pp. 275–287, 2016.

[12] J. A. García-Grajales, A. Jérusalem, and A. Goriely, "Continuum mechanical modeling of axonal growth," *Computer Methods in Applied Mechanics and Engineering*, vol. 314, pp. 147–163, 2017.

[13] S. C. Gupta, *The classical Stefan problem: basic concepts, modelling and analysis with quasi-analytical solutions and methods*. Elsevier, 2017, vol. 45.

[14] W. P. Heemels, K. H. Johansson, and P. Tabuada, "An introduction to event-triggered and self-triggered control," in *2012 ieee 51st ieee conference on decision and control (cdc)*. IEEE, 2012, pp. 3270–3285.

[15] W. Heemels, J. Sandee, and P. Van Den Bosch, "Analysis of event-driven controllers for linear systems," *International journal of control*, vol. 81, no. 4, pp. 571–590, 2008.

[16] E. A. Huebner and S. M. Strittmatter, "Axon regeneration in the peripheral and central nervous systems," *Cell biology of the axon*, pp. 305–360, 2009.

[17] M. Izadi, J. Abdollahi, and S. S. Dubljevic, "PDE backstepping control of one-dimensional heat equation with time-varying domain," *Automatica*, vol. 54, pp. 41–48, 2015.

[18] E. Kofman and J. H. Braslavsky, "Level crossing sampling in feedback stabilization under data-rate constraints," in *Proceedings of the 45th IEEE Conference on Decision and Control*. IEEE, 2006, pp. 4423–4428.

[19] S. Koga, C. Demir, and M. Krstic, "Event-triggered safe stabilizing boundary control for the stefan pde system with actuator dynamics," in *2023 American Control Conference (ACC)*. IEEE, 2023, pp. 1794–1799.

[20] M. Krstic, "Compensating actuator and sensor dynamics governed by diffusion PDEs," *Systems & Control Letters*, vol. 58, no. 5, pp. 372–377, 2009.

[21] M. Krstic and A. Smyshlyaev, *Boundary control of PDEs: A course on backstepping designs*. SIAM, 2008.

[22] X. Z. Liu, X. M. Xu, R. Hu, C. Du, S. X. Zhang, J. W. McDonald, H. X. Dong, Y. J. Wu, G. S. Fan, M. F. Jacquin *et al.*, "Neuronal and glial apoptosis after traumatic spinal cord injury," *Journal of Neuroscience*, vol. 17, no. 14, pp. 5395–5406, 1997.

[23] R. B. Maccioni, J. P. Muñoz, and L. Barbeito, "The molecular bases of Alzheimer's disease and other neurodegenerative disorders," *Archives of medical research*, vol. 32, no. 5, pp. 367–381, 2001.

[24] D. R. McLean, A. van Ooyen, and B. P. Graham, "Continuum model for tubulin-driven neurite elongation," *Neurocomputing*, vol. 58, pp. 511–516, 2004.

[25] B. Rathnayake and M. Diagne, "Event-based boundary control of one-phase stefan problem: A static triggering approach," in *2022 American Control Conference (ACC)*. IEEE, 2022, pp. 2403–2408.

[26] ——, "Event-based boundary control of the stefan problem: A dynamic triggering approach," in *2022 IEEE 61st Conference on Decision and Control (CDC)*. IEEE, 2022, pp. 415–420.

[27] ——, "Observer-based periodic event-triggered boundary control of the one-phase stefan problem," *IFAC-PapersOnLine*, vol. 56, no. 2, pp. 11 415–11 422, 2023.

[28] ——, "Periodic event-triggered boundary control of a class of reaction-diffusion pdes," in *2023 American Control Conference (ACC)*. IEEE, 2023, pp. 1800–1806.

[29] ——, "Self-triggered boundary control of a class of reaction-diffusion pdes," in *2023 62nd IEEE Conference on Decision and Control (CDC)*. IEEE, 2023, pp. 6887–6892.

[30] L. Squire, D. Berg, F. E. Bloom, S. Du Lac, A. Ghosh, and N. C. Spitzer, *Fundamental neuroscience*. Academic press, 2012.

[31] G. A. Susto and M. Krstic, "Control of pde–ode cascades with neumann interconnections," *Journal of the Franklin Institute*, vol. 347, no. 1, pp. 284–314, 2010.

[32] S. Tang and C. Xie, "State and output feedback boundary control for a coupled pde–ode system," *Systems & Control Letters*, vol. 60, no. 8, pp. 540–545, 2011.

[33] M. P. Van Veen and J. Van Pelt, "Neuritic growth rate described by modeling microtubule dynamics," *Bulletin of mathematical biology*, vol. 56, no. 2, pp. 249–273, 1994.

[34] H. Yu, M. Diagne, L. Zhang, and M. Krstic, "Bilateral boundary control of moving shockwave in lwr model of congested traffic," *IEEE Transactions on Automatic Control*, 2020.